Discover Oncology

Research

Comprehensive analysis Neddylation-related genes identified UBB as a prognostic biomarker for clear cell renal cell carcinoma

Shengren Cen[1] · Yingpeng Li[1] · Xinhao Xiong[1] · Zihong Ma[1] · Yongsheng Wang[1] · Xingcheng Gao[1]

Received: 13 September 2024 / Accepted: 2 May 2025
Published online: 22 May 2025

Abstract
Neddylation, as a type of post-translational modification, plays a key role in cancer development. However, the biological characteristics and clinical prognosis value of Neddylation-related genes (NRGs) signatures in clear cell renal cell carcinoma (ccRCC) remain undetermined. Here, we identified two subtypes of NRGs in ccRCC based on TCGA data and constructed a NRGs risk signature (NRGS). Survival analysis, ROC curves, and nomograms showed that NRGS was an important predictor of prognosis in patients with clear cell renal cell carcinoma. We further revealed important correlations between NRGS and clinicopathological features, gene mutations, drug sensitivity, and immune cell infiltration. High NRGS indicates a poorer prognosis for kidney cancer, but higher remission rates with immunotherapy. Drug sensitivity also varies across risk groups. UBB was identified as a hub gene for NRGS and was downregulated in ccRCC, which is associated with poor prognosis. In conclusion, this study provides strategies for predicting prognosis and individualizing treatment for ccRCC.

Keywords Clear cell renal cell carcinoma · Neddylation · Immune environment · Drug sensitivity · Prognosis · UBB

1 Introduction

According to U.S. cancer statistics, the number of new estimated cases of kidney and renal pelvis-related cancers is increasing each year. Clear cell renal cell carcinoma (ccRCC) is the most common type of kidney cancer and is the leading cause of kidney cancer-related deaths [1–3]. Although localized ccRCC can be treated by surgical resection or ablation, treatment options for advanced disease are limited by resistance to radiotherapy and chemotherapy, making the search for new therapeutic targets a priority. Therapeutic combinations such as immune checkpoint inhibitors (e.g., pembrolizumab) in combination with tyrosine kinase inhibitors (e.g., axitinib) have been shown to be practicable [4–6]. However, the impact of these treatments on tumor suppression and patient survival varies, suggesting the need for new regimens to improve patient prognosis.

Shengren Cen, Yingpeng Li, and Xinhao Xiong contributed equally.

Supplementary Information The online version contains supplementary material available at https://doi.org/10.1007/s12672-025-02547-7.

✉ Xingcheng Gao, xchgao@gzhmu.edu.cn; Shengren Cen, 360541005@qq.com; Yingpeng Li, 1074943052@qq.com; Xinhao Xiong, 2714651325@qq.com; Zihong Ma, 1137879252@qq.com; Yongsheng Wang, 1285486484@qq.com | [1]Guangdong Provincial Key Laboratory of Urological Diseases, Guangzhou Institute of Urology, Department of Urology, The First Affiliated Hospital of Guangzhou Medical University, Guangzhou 510230, Guangdong, China.

Post-translational modifications are covalent modifications of proteins after biosynthesis, usually enzymatic. Post-translational modifications are involved in many biological processes, not only regulating protein degradation, but also regulating oncogenic signaling, etc., thus have received increasing attention in cancer research [7, 8]. Neddylation, a type of post-transcriptional modification, plays an important role in the development of cancer, as a result, there is increasing interest in developing therapies that can specifically utilize ubiquitin and ubiquitin-like pathways to treat cancer. Neddylation is a specific modification of the binding of the ubiquitin-like protein NEDD8 to a substrate protein and consists of a series of enzymatic reactions. Enzymes that regulate Neddylation include NEDD8 activase (E1), NEDD8 conjugating enzyme (E2), and NEDD8 ligase (E3) [9]. In addition to basic functions in proteome degradation and recycling, Neddylation is involved in epithelial-mesenchymal transition, transcriptional regulation, and cell death regulation [10]. In breast cancer, HER2 is neddylated, which prevents its degradation and thus promotes breast cancer development; therefore, inhibition of Neddylation and combination with trastuzumab may be a strategy to inhibit HER2-positive breast cancer progression [11]. Zhou et al. reported that MLN4924 inhibits Neddylation by inactivating CRL3-SPOP E3 ligase, which protects the glutamine transporter ASCT2/SLC1A5 from degradation, thereby enhancing glutamine intake by breast cancer cells [12]. These studies further confirm that targeting Neddylation may be a strategy for tumor therapy. In renal cancer, Neddylation inhibition sensitizes renal medullary carcinoma tumor to platinum chemotherapy, which works by inhibiting P53-induced DNA damage repair and increasing apoptosis in renal medullary carcinoma cells [13]. Inhibition of Neddylation modification triggers DNA damage, inhibits cell growth, and suppresses the migratory and invasive capacity of clear cell renal carcinoma by regulating E-cadherin and Vimentin expression [14]. These findings suggest that Neddylation is essential for the growth of ccRCC. However, the biological functions and mechanisms of Neddylation modification in the pathogenesis of ccRCC remain unclear and need to be further elucidated. In addition, mechanisms of protein homeostasis associated with Neddylation have not yet been studied as potential biomarkers of drug efficacy or prognosis in ccRCC [7]. A comprehensive investigation of Neddylation-related genes (NRGs) may help to develop rational diagnostic and therapeutic strategies for ccRCC.

In the current study, we downloaded transcriptome data and clinical information about ccRCC from TCGA and genes related to Neddylation from online databases. Next, we assessed the DEGs of NRGs across ccRCC tissues and normal tissues. Using these genes, we divided the patients into two groups with the help of "ConsensusClusterPlus" package and analyzed the differences between the two groups. A six Neddylation-related genes signature were then constructed by applying Lasso and multivariate Cox regression analysis. Combining the NRGs risk score and clinical parameters, we also constructed a nomogram to predict prognosis. Besides, we categorized the patients into two subgroups based on the median NRGs risk score and noted significant differences between the two subgroups in terms of TME components, somatic mutations, immune checkpoint expression profiles, and drug responses. We also found that low expression levels of UBB predicted a poorer prognosis. In conclusion, these findings indicate that Neddylation-related genes are important in the development of ccRCC, and elucidating the key role of NRGs may ultimately lead to better treatment options for ccRCC patients.

2 Materials and methods

2.1 Data collection and process

Transcriptome profiles and clinical information for ccRCC were obtained from online database TCGA (https://portal.gdc.cancer.gov) by utilizing the R package "TCGAbiolinks". E-MTAB-1980 queue is available from the online database EMBL-EBI (https://www.ebi.ac.uk/). TCGA-ccRCC clinical data were screened by (1) Follow-up time ≥30 days and (2) excluding samples without complete OS clinical information. A total of 516 ccRCC patients were included. Differentially expressed genes (DEGs) between tumor tissues and normal tissues were identified utilizing the "Limma" package on the R platform. adj. *P*.val < 0.05,|Log2FC|≥ 0.6 was regarded as statistically significant. Neddylation-related genes (Supplementary Table 1) were obtained from the Reactome (https://reactome.org/), GSEA (https://www.gsea-msigdb.org/gsea/msigdb), and GeneCards (https://www.genecards.org/) databases (relevance score ≥ 1). The ccRCC scRNA-seq dataset (GSE159115) was available from the online database Gene Expression Omnibus (GEO) (https://www.ncbi.nlm.nih.gov/gds/?term=GSE159115), and analyzed using the online tool SolvingLab (http://solvinglab.com.cn/).

2.2 Functional enrichment analysis

Differentially expressed genes were applied to perform Gene Ontology (GO), Kyoto Encyclopedia of Genes and Genomes (KEGG) and gene set enrichment analysis (GSEA) using "ClusterProfiler" package [15]. "GSVA" was accepted to carry out Gene Set Variation Analysis.

2.3 Consensus clustering analysis

Based on differentially expressed Neddylation-related genes, unsupervised hierarchical clustering of the TCGA-ccRCC dataset was performed utilizing the "ConsensusClusterPlus" package to identify Neddylation-associated molecular isoforms [16]. 1000 iterations were performed to insure the robustness of each clustering. The optimum number of clusters was derived using the "proportion of ambiguous clustering" (PAC), with the lowest PAC for K values.

2.4 Prognostic model construction

The 111 Neddylation-associated DEGs were chosen for performing univariate Cox regression analysis. Next, the prognostic genes were utilized to conduct the Least Absolute Shrinkage and Selection Operator (LASSO) Regression analysis, and select the minimum penalty term by tenfold cross validation. Then using multivariate Cox regression and stepwise regression analyses and following Akaike information criterion (AIC), we derived a Neddylation-related gene signature (NRGS). The risk score of NRGS was measured as formula: risk_score = $\sum_{i=1}^{n}$ (Coefi × Expi); Coefi represents the relevant regression coefficient and Expi represents the expressed value of NRGs. According to the median risk score, we categorized patients into two different groups. Receptor operator characteristic curves (ROCs) was applied to assess the prognosis of the 1-, 3-, and 5-year OS in TCGA- ccRCC, which was validated by applying E-MTAB-1980 dataset.

2.5 Drug response prediction

Drug responses were estimated using the Genomics of Drug Sensitivity in Cancer (GDSC) [17] containing 809 cell lines and 198 compounds using the "oncoPredict" software package [18]. Half-maximal inhibitory concentrations (IC50) were calculated for patients between the two risk groups using a ridge regression model.

2.6 Somatic mutation analysis

The total somatic mutation burden between different risk score subgroups of TCGA- ccRCC was estimated using the R package "TCGAmutations". The Waterfall diagram was drawn utilizing the online website Sangerbox [19] to show the mutations between the different groups.

2.7 Construction of Nomogram

Nomograms predicting the prognosis of 1-, 3-, and 5-year overall survival of ccRCC suffers according to the TCGA-ccRCC dataset were plotted using the "rms" software package based on the NRGs risk score and other relevant clinical parameters. Decision curve and calibration curve were conducted to confirm the clinical credibility of this Nomogram model.

2.8 Analysis of the tumor immune microenvironment

The R packages "ESTIMATE", "MCPcounter" and "CIBERSORT" were used to predict immunity scores, ESTIMATE score and immune cell infiltration. Six NRGS genes were assessed for correlation with lymphocytes using the online website: TIMER (Tumor Immune Estimation Resouse). In addition, the expression of common immune checkpoints (TIGIT, IDO1, CD274,

CD276, CD44, PDCD1LG2, PDCD1, CTLA4, LAG3) was analyzed between the two groups. Predicting immunotherapy response using the IMvigor210 renal cancer cohort (http://research-pub.gene.com/IMvigor210CoreBiologies/).

2.9 Cell culture

RCC cell lines 786-O and ACHN were obtained from the Stem Cell Bank of the Chinese Academy of Sciences.786-O and ACHN were cultured in 1640 medium containing 10% FBS, and the cell lines were cultured in a humidified environment at 37 °C with 5% CO_2.

2.10 Transfection and RT-qPCR

The UBB plasmid vector was constructed by inserting the full-length cDNA of UBB into the pcDNA3.1 vector: CMV-MCS-3fag-polyA-EF1A-zsGreen-sv40-puromycin. Lipofectamine 3000 was purchased from Invitrogen (L3000015) and used for transfection of the plasmid according to the manufacturer's recommendations. Total RNA was extracted using TRIzol reagent (Invitrogen, USA), reverse transcribed using a PrimeScript RT kit (Takara, Japan), and quantified by qRT-PCR using SYBR green (Takara, Japan) on a Bio-Rad CFX96 system. The expression of UBB was normalized to β-actin (mRNA) using the2−ΔΔCt method.

2.11 Cell proliferation

Cell proliferation was detected using the Cell Counting Kit-8 (K1018-5 ml, APEXBIO) according to the manufacturer's instructions. Briefly, cells were cultured in 96-well plates (2000 cells/well). After cell attachment, add 100ul of serum-free medium containing 10% CCK-8 to each well and incubate for 2 h at 37 °C in an incubator. Finally, the optical density (OD) at 450 nm was detected using a microplate reader (EXL800, BioTek Instruments).

2.12 Statistical analyses

Statistical analysis was carried out on the platform R 4.1.3 (https://www.r-project.org/). Continuous variables were utilized to analyze the Mann–Whitney-Wilcoxon test. Using the "Survival" package, log-rank test computations were used to generate Kaplan–Meier survival curves. Spearman's correlation analysis was used to test the correlation analysis. *P*-value ≤ 0.05 was taken as the threshold for statistical significance.

3 Results

3.1 Identification of two distinct patterns of ccRCC based on Neddylation-related genes

To identify features of Neddylation-related genes, we collected 504 NRGs from the GSEA database, Reactome database and GeneCards (correlation score ≥ 1). We then assessed the DEGs of TCGA-ccRCC dataset. As illustrated in Fig. 1A, 111 differentially expressed genes were obtained. Enrichment analyses showed that these differentially expressed NRGs are involved in the progression of various cancers and are mainly enriched in regulating the proteasome and ubiquitin-like related protein activity (Fig. 1B, C). Furthermore, based on the 111 DEGs associated with Neddylation, we divided ccRCC patients into multiple subgroups using consensus clustering (Fig. 1D). Determination of the optimal k-value using the Cumulative Distribution Function and the PAC algorithm (Fig. 1E, F). As shown in the tSNE plot, patients with ccRCC based on NRGs can be well categorized into two groups (Fig. 1G). We further analyzed the survival rates of the two clusters and found that the prognosis of cluster 2 is poorer (Fig. 1H).

3.2 Differences in tumor microenvironment and biological function between the two clusters

To investigate the characteristics between the two clusters, we analyzed the DEGs between clusters using the limma package. We got 265 differentially expressed genes (|logFC|≥ 1, $P < 0.05$) (Fig. 2A). GO term analysis was utilized to evaluate the biological functions of these differentially expressed genes. The results indicated that these DEGs participate in energy derivation by oxidation of organic compounds, apical part of cell, and endopeptidase

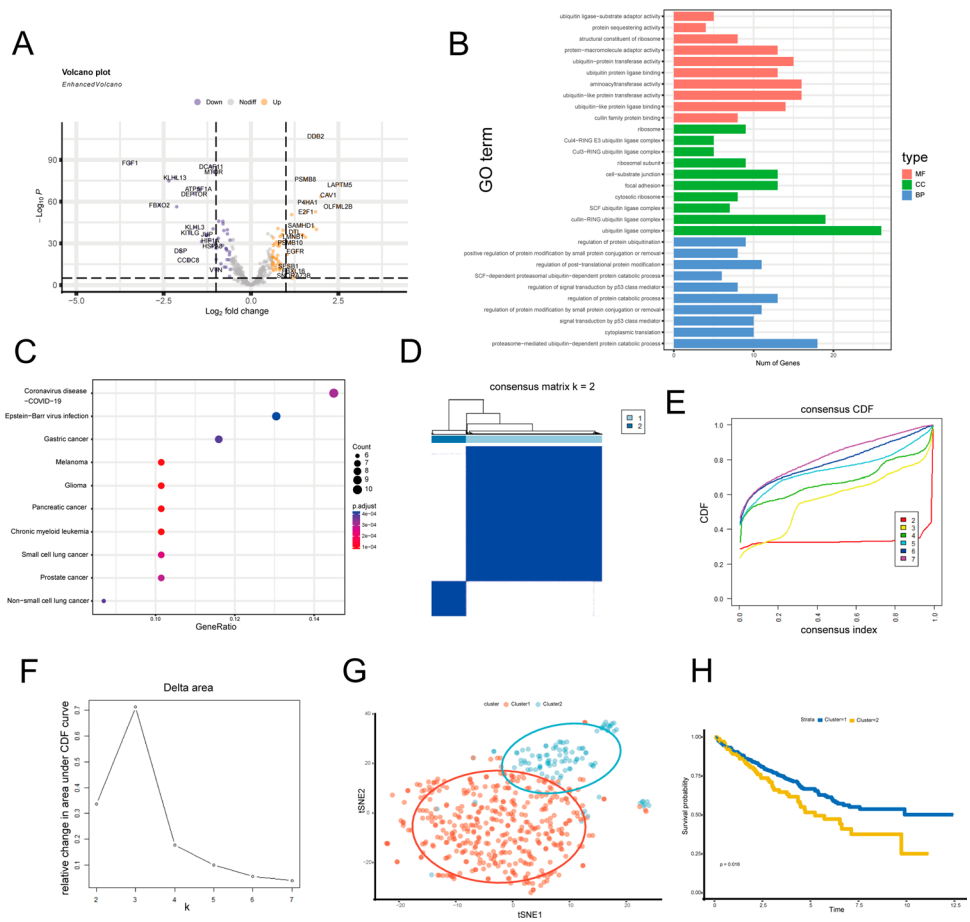

Fig. 1 Characterization of Neddylation-related genes and patterns of NRGs in ccRCC. **A** Volcano map of differentially expressed NRGs in the TCGA dataset. **B** Enrichment of GO terms for Neddylation-related DEGs. **C** Dot plot showing KEGG pathway enrichment of Neddylation DEGs. **D** Consensus matrices of the TCGA-ccRCC cohort for k = 2. **E** Consensus values range from 0 to 1. **F** The corresponding area under the cumulative distribution function (CDF), optimal k = 2. **G** tSNE analysis of the two subgroups. **H** Survival analysis of patients between cluster-1 and cluster-2

regulator activity (Fig. 2B). Furthermore, KEGG and GSEA revealed that these DEGs involve in various cancer related pathways, including Oxidative phosphorylation, Cell adhesion molecules, and Focal adhesion (Fig. 2C, D). In order to identify the potential mechanisms that may explain the differences between the two subsets, we further conducted GSVA. Remarkably, many of the signaling pathways involved in oncogenesis and intercellular communication are altered, including adherens junctions, oxidative phosphorylation, and tyrosine metabolism (Fig. 2E, F). To further characterize the immune profile of different NRGs patterns, we estimated the immune infiltration profile of immune cell ratios by ssGSEA analysis. Compared to Cluster 2, the infiltration levels of immunocytes in Cluster 1(such as macrophages and activated CD4 T cells) are significantly higher (Fig. 2G, H). This suggests that the response to immunotherapy may differ between these two clusters, which has significant implications for the clinical practice and research of ccRCC.

3.3 Construction of Neddylation-related genes prognostic signature

In order to further analyze the potential prognostic function of NRGs, we established a prognostic signature. Based on 111 NRGs, with the assistance of univariate Cox regression analysis and lasso regression analysis, we generated 12 genes according to the least partial likelihood bias (Fig. 3A, B). Next, prognostic risk was modeled for these six genes using the Akaike Information Criterion (AIC) in multivariate Cox regression analysis (Fig. 3C). Based on the risk model, the patients with clear cell renal cancer was separated into two subsets according to the median risk score (Fig. 3D). We used the ROC curve to evaluate the predictive value of the risk model, with areas under the ROC curve at 1, 3, and 5 years being 0.756, 0.722, and 0.763, respectively (Fig. 3E). In addition, compared to the high-risk group, K-M plot shows that the low-risk group has a better prognosis (Fig. 3F). These findings indicated that the model performs well in predicting the prognosis of ccRCC.

Fig. 2 Molecular characterization and immune cells of different NRGs subgroups. **A** Volcano plot of DEGs between two subgroups in the TCGA dataset. **B**, **C** Dot plot showing GO and KEGG pathway enrichment of DEGs. **D** Top 5 GSEA results between Cluster 1 and 2. **E**, **F** KEGG pathway analysis of GSVA in two subgroups. **G** The ssGSEA analysis of the immune cell infiltration level in the two subgroups. **H** Boxplot of the abundance of immune cells in the two subgroups. *$P < 0.05$, **$P < 0.01$, ***$P < 0.001$, *ns* not significant

3.4 Establishment of nomograms combining clinical factors and risk scores

To evaluated the clinical function of NRGs risk scores in ccRCC, the relationship between risk score and clinical characteristics was assessed. We found a positive correlation between the risk score and tumor stage; the higher tumor the grade, the higher the risk score (Fig. 4A, B). The risk score for males is higher than that for females (Fig. 4C). Furthermore, using univariate and multivariate Cox regression analysis, we verified that the NRGs risk score is an independent prognostic factor for ccRCC, as confirmed by the E-MTAB-1980 dataset (Fig. 4D, E, S1). To better predict the survival rate of ccRCC patients, we created a nomogram using tumor stage, Gender, Age, and NRGs risk scores of ccRCC patients (Fig. 4F). The calibration curve was used to assess the consistency between the predicted probabilities and the actual probabilities of occurrence of this nomogram, we found that the predicted probabilities closely match the actual probabilities (Fig. 4G). The ROC curve also indicates that the nomogram has good performance in predicting survival rates (Fig. 4H). The DCA curve further confirms the good predictive efficacy of the nomogram (Fig. 4I).

3.5 The potential functional mechanisms between different risk groups

In order to clarify the potential mechanisms in different groups, DEGs were calculated using "Limma" package. 222 differentially expressed genes ($|\log FC| \geq 1$, $P < 0.05$) (Fig. 5A) were used to perform GO term enrichment analysis. The results showed that these DEGs are primarily involved in immunoglobulin production, immunoglobulin complexes, and antigen binding (Fig. 5B). KEGG and GSEA analyses further revealed that these DEGs are primarily involved in primary immunodeficiency, cytokine-cytokine receptor interaction, and fatty acid metabolism (Fig. 5C, D). In addition, GSVA showed that these DEGs in the risk signature focused on fatty acid metabolism, primary immunodeficiency, and citrate cycle TCA cycle (Fig. 5E). To explore the immune characteristics of NRGs risk types, we detected the relationship between tumor microenvironment (TME) and NRGs risk score through ssGSEA. The findings indicated that, compared to the low-risk group, the overall infiltration level of TME cells in the high-risk group is significantly higher (Fig. 5F). All of this suggests that these two risk subtypes have distinct biological characteristics and immune microenvironments, and may identify new therapeutic targets due to these differences.

3.6 Predicting immune infiltration and gene mutations based on risk scores

We further analysed the frequencies of somatic mutated genes in different risk groups. Among the top five genes, there were remarkable differences in the mutation frequencies of PBRM1, BAP1, and ARIDIA (Fig. 6A, B). The two groups of genes have different mutation frequencies, which may account for the functional differences between the two groups. In addition, compared to the low-risk group, the total mutational burden (TMB) was higher in the high-risk group (Fig. 6C). Mutations in cellular genes produce new antigens that lead to changes in the infiltration level of immunocytes in tumor tissue. Using the ESTIMATE algorithm, we discovered that the scores of estimation, stromal and immune are higher in the high-risk group (Fig. 6D–F). MCPcounter found that the infiltration levels of lymphocytes (such as T-cell B lymphocytes) are higher in high-risk group (Fig. 6G). CIBERSORT analysis also showed that the levels of lymphocyte infiltration differ between these two risk groups (Fig. 6H, S2). To better understand the association between NRGS and immune cell infiltration, we analyzed six NRGS genes and lymphocyte infiltration using TIMER and found that tumor lymphocyte infiltration levels were positively correlated with gene expression (Fig. S3). In summary, these finding indicated that the differences in prognosis and biological functions among different groups may be related to distinct tumor microenvironments, which may guide the search for new potential therapeutic approaches.

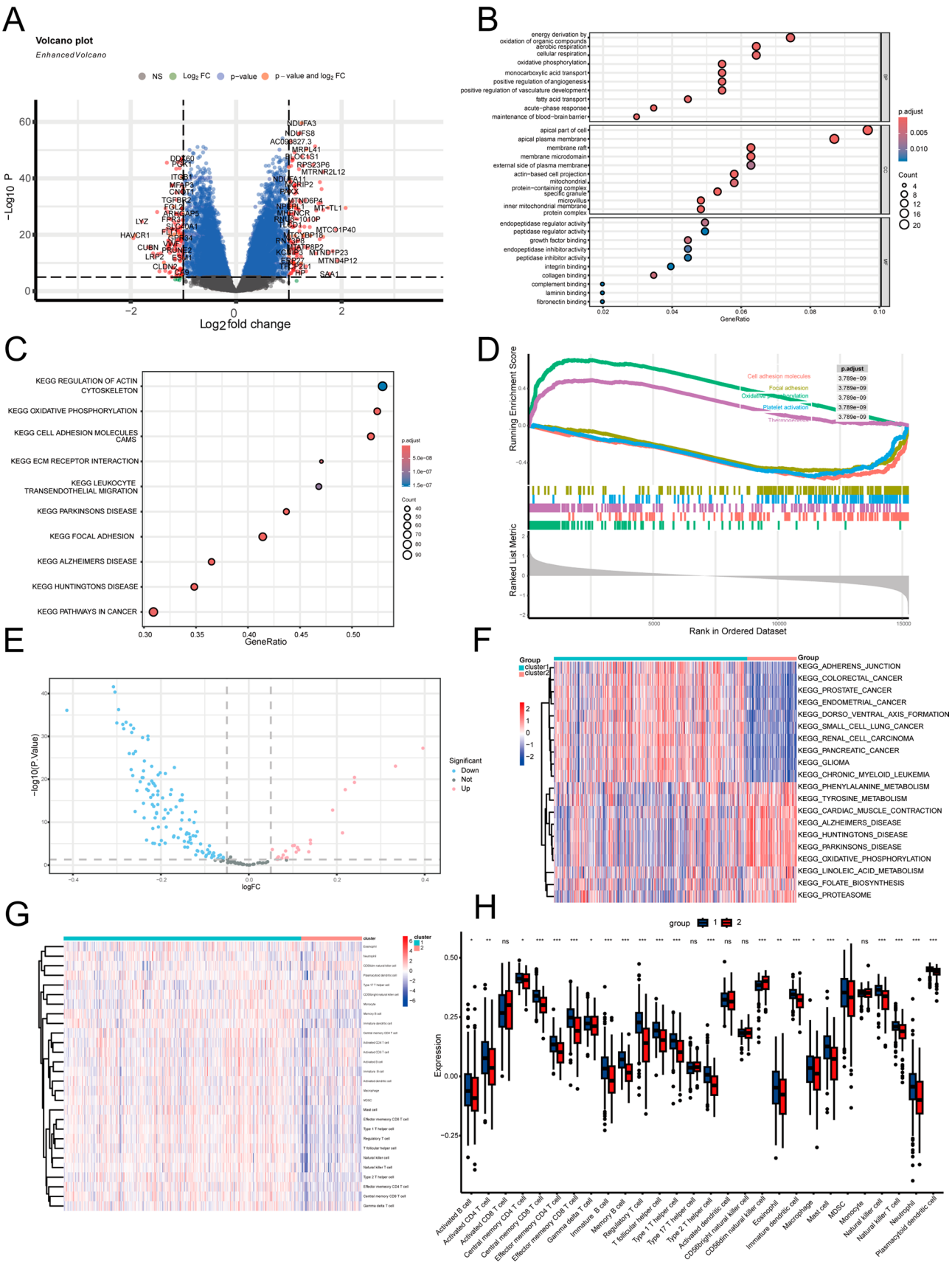
A
Volcano plot
Enhanced Volcano
NS
Log2 FC
p-value
p - value and log2 FC
−Log10 P
Log2 fold change
B
energy derivation by oxidation of organic compounds
aerobic respiration
cellular respiration
oxidative phosphorylation
monocarboxylic acid transport
positive regulation of angiogenesis
positive regulation of vasculature development
fatty acid transport
acute−phase response
maintenance of blood−brain barrier
apical part of cell
apical plasma membrane
membrane raft
membrane microdomain
external side of plasma membrane
actin−based cell projection
mitochondrial protein−containing complex
specific granule
microvillus
inner mitochondrial membrane protein complex
endopeptidase regulator activity
peptidase regulator activity
growth factor binding
endopeptidase inhibitor activity
peptidase inhibitor activity
integrin binding
collagen binding
complement binding
laminin binding
fibronectin binding
p.adjust
Count
GeneRatio
C
KEGG REGULATION OF ACTIN CYTOSKELETON
KEGG OXIDATIVE PHOSPHORYLATION
KEGG CELL ADHESION MOLECULES CAMS
KEGG ECM RECEPTOR INTERACTION
KEGG LEUKOCYTE TRANSENDOTHELIAL MIGRATION
KEGG PARKINSONS DISEASE
KEGG FOCAL ADHESION
KEGG ALZHEIMERS DISEASE
KEGG HUNTINGTONS DISEASE
KEGG PATHWAYS IN CANCER
p.adjust
Count
GeneRatio
D
Cell adhesion molecules
Focal adhesion
Oxidative phosphorylation
Platelet activation
Thermogenesis
p.adjust
Running Enrichment Score
Ranked List Metric
Rank in Ordered Dataset
E
−log10(P Value)
logFC
Significant
Down
Not
Up
F
Group
cluster1
cluster2
KEGG_ADHERENS_JUNCTION
KEGG_COLORECTAL_CANCER
KEGG_PROSTATE_CANCER
KEGG_ENDOMETRIAL_CANCER
KEGG_DORSO_VENTRAL_AXIS_FORMATION
KEGG_SMALL_CELL_LUNG_CANCER
KEGG_RENAL_CELL_CARCINOMA
KEGG_PANCREATIC_CANCER
KEGG_GLIOMA
KEGG_CHRONIC_MYELOID_LEUKEMIA
KEGG_PHENYLALANINE_METABOLISM
KEGG_TYROSINE_METABOLISM
KEGG_CARDIAC_MUSCLE_CONTRACTION
KEGG_ALZHEIMERS_DISEASE
KEGG_HUNTINGTONS_DISEASE
KEGG_PARKINSONS_DISEASE
KEGG_OXIDATIVE_PHOSPHORYLATION
KEGG_LINOLEIC_ACID_METABOLISM
KEGG_FOLATE_BIOSYNTHESIS
KEGG_PROTEASOME
G
cluster
H
group
Expression
Activated B cell
Activated CD4 T cell
Activated CD8 T cell
Central memory CD4 T cell
Central memory CD8 T cell
Effector memory CD4 T cell
Effector memory CD8 T cell
Gamma delta T cell
Immature B cell
Memory B cell
Regulatory T cell
T follicular helper cell
Type 1 T helper cell
Type 17 T helper cell
Type 2 T helper cell
Activated dendritic cell
CD56bright natural killer cell
CD56dim natural killer cell
Eosinophil
Immature dendritic cell
Macrophage
Mast cell
MDSC
Monocyte
Natural killer cell
Natural killer T cell
Neutrophil
Plasmacytoid dendritic cell

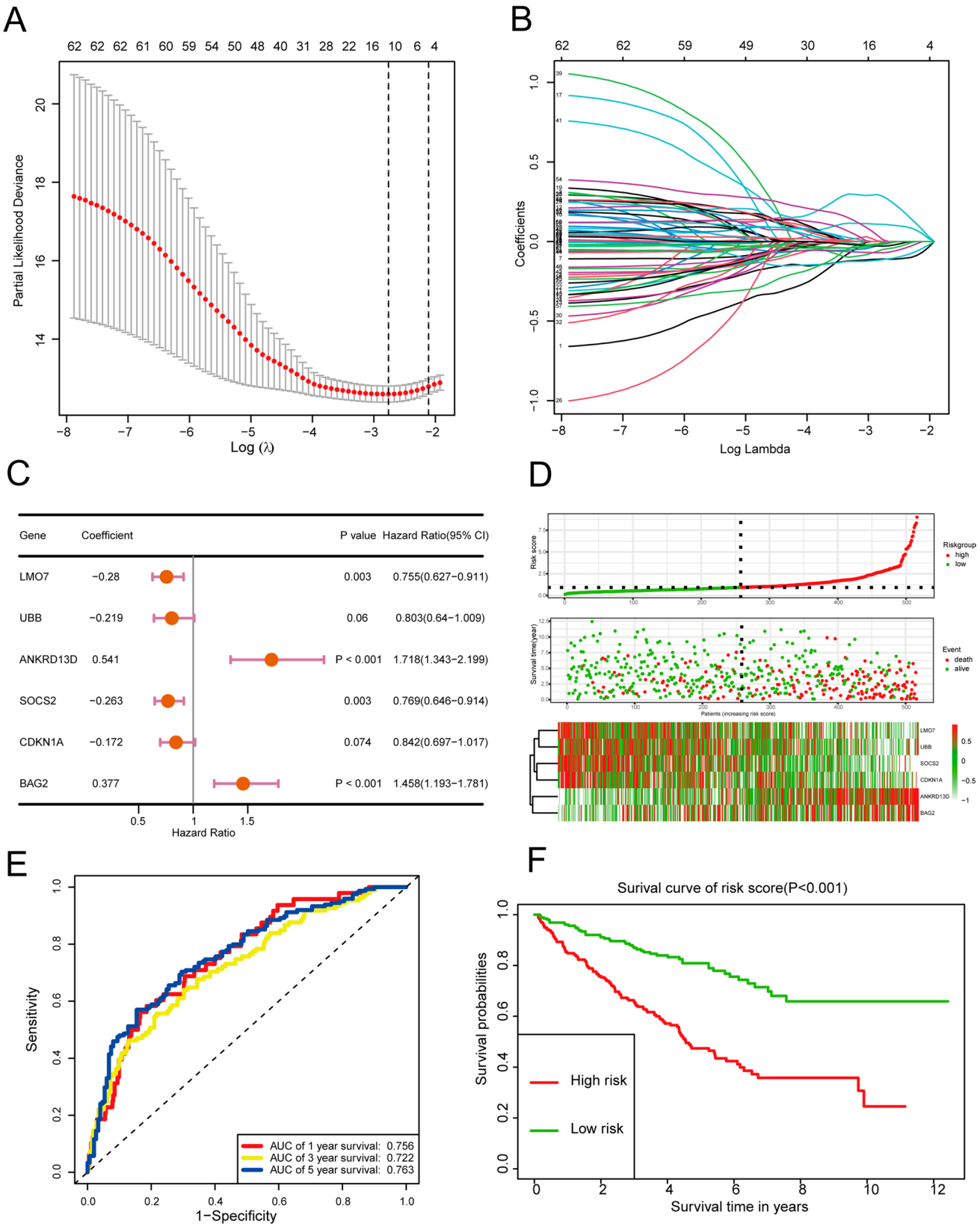

Fig. 3 Construction of NRGs prognostic risk score model. **A** Neddylation-related genes were penalized by LASSO Cox regression analysis. **B** Ten-fold cross-validation for the optimal parameter selection in the LASSO Cox regression. **C** A six-gene model was constructed by stepwise regression modeling using the Akaike Information Criteria (AIC) method. **D** Risk score distribution, OS status, and six-gene expression trends in the TCGA ccRCC dataset. **E** ROC curves for the performance of prognostic models in the ccRCC dataset at 1, 3, and 5 years over time. **F** Kaplan–Meier survival analysis of NRGS in ccRCC

3.7 Predicting immunotherapy response and drug sensitivity

Since we found that NRGS risk scores correlated with immunocyte infiltration, we sought to determine the association between NRGS risk scores and immune responses. We utilized the CIBERSORT algorithm to evaluate several common immune checkpoints. In the correlation analysis, we found a positive correlation between the expression of immune checkpoints and risk score. The high-risk group had higher levels of expression of most immune checkpoints compared to the low-risk group (Fig. 7A, B), meaning that the high-risk group may be more sensitive to immune checkpoint inhibitors. Using the IMvigor210 cohort, we analyzed the responses to immunotherapy among different NRGS risk groups and determined that the NRGS risk scores for renal cancer in the CR/PR group were higher. However, the statistical results were not significant, which may be related to the sample size. In addition, combined with immunotherapy, the prognosis of the high-risk group was better (Fig. 7C, D). Since chemotherapy is one of the clinical treatment options for patients with ccRCC, we calculated the IC50 values of several chemotherapy drugs based on the GDSC database to assess chemotherapy sensitivity through the pRRophetic package and compared the IC50 values between the two risk groups. The results showed that Epirubicin, Cytarabine, Docetaxel, and Cisplatin had significantly lower estimated IC50 values in the high-risk group (Fig. 7E–H), suggesting that high-risk groups may be more susceptible to the effects of these drugs. In the correlation analysis, we found that NRGS risk score related to drug susceptibility was associated with DNA replication (Leflunomide, Pyridostatin and topotecan) and WNT singling pathway (WIKI4 and XAV939), etc. Drug resistant to NRGS risk score was associated with cell cycle (RO-3306), Chromatin histone acetylation (OF-1), and RTK (SB505124) (Fig. 7I, J).

3.8 Identification of NRGS hub gene UBB

Using the "mgeneSim" algorithm, we found that UBB is a hub gene of NRGS [20] (Fig. 8A). By analyzing the TCGA-ccRCC dataset, we found that UBB was downregulated in ccRCC (Fig. 8B, C), and low UBB expression was associated with poorer disease-free survival and overall survival (Fig. 8D, E), suggesting that UBB may play a key role in cancer progression. Meanwhile, we found that the methylation of the UBB promoter was upregulated in renal cancer, which may be responsible for the downregulation of UBB in ccRCC (Fig. 8F). In addition, the expression of UBB in the ccRCC-immunized microenvironment was determined using the ccRCC single-cell dataset (GSE159115). The results showed that UBB was mainly highly expressed in pericytes and endothelial cells, and less in malignant cells in the microenvironment (Fig. 8G–I). CCK8 assays showed inhibition of kidney cancer cell proliferation after overexpression of UBB (Fig. 8J–L). This result is consistent with the finding that UBB mediates resistance to pazopanib by modulating angiogenesis in ccRCC [21]. These results demonstrate that UBB plays a critical role in renal cancer and warrants further investigation.

4 Discussion

ccRCC is a common urologic tumor with an insidious onset, and approximately 25–30% of patients already have metastases at diagnosis. Although the 5-year relative survival rate for ccRCC improves with improved treatment, the overall prognosis remains unsatisfactory [22–24]. Therefore, it is worthwhile to find new prognostic biomarkers for diagnosis and individualized treatment. Previous studies have shown that post-translational modifications play a key role in several activities such as cell death, cell metabolism, and cancer development. The mechanisms are widely recognized for their effects on human disease. With the understanding of the mechanism of post-translational modification, scholars have been able to molecularly classify a variety of cancer types and construct prognostic models [25, 26]. Nevertheless, the clinical significance and prognostic potential of Neddylation-related genes in ccRCC are still largely unexplored.

In this study, a bioinformatics investigation was performed to systematically study the biological function and clinical relevance of NRGs in ccRCC. We developed a risk model that included six Neddylation-related genes: LMO7, UBB, ANKRD13D, SOCS2, CDKN1A, and BAG2. Significant differences in biological characteristic were observed in different risk groups. Of these six genes, LMO7 (LIM structural domain-only protein 7) is expressed in a variety of tissues and cells and is involved in multiple processes, such as maintenance of epithelial structure, ubiquitination, and macrophage polarization and metabolism [27, 28]. This indicates that LMO7 may function in the ccRCC process by affecting cell adhesion and immune cell regulation. UBB, or ubiquitin B, has an influential function in the targeted

Fig. 4 Correlations between risk models and clinical characteristics based on the TCGA ccRCC dataset. Violin plot shows different NRGs risk score between different pathological stage (**A**), clinical staging (**B**), and gender (**C**). Univariate (**D**) and multivariate (**E**) Cox regression analysis were used to explore the prediction of NRGs risk. **F** Nomogram predicting the probability of patient survival using NRG-related risk scores, age, sex, p_staging, and staging. **G** The calibration curves of the nomogram. **H** ROC curve of the prognostic model. **I** Decision curve analysis (DCA) of the nomogram

degradation of cellular proteins and is involved in many biological functions [29, 30]. Studies have shown that UBB can affect angiogenesis by regulating vascular endothelial growth factor through direct interaction with SP1 [21]. Consistent with this study, we found that UBB was downregulated in ccRCC and higher UBB expression was associated with better prognosis, suggesting that UBB is a protective factor. We also found that UBB is relatively highly expressed in pericytes and endothelial cells, which are critical for cancer angiogenesis. The critical function of UBB in pericytes and endothelial cells deserves a step forward. ANKRD13D (ankrin repeat structural domain 13D) is a member of the ankrin repeat structural domain (ANKRD) 13 family, which binds specifically to the ubiquitin chain attached to Lys-63 on membrane-bound proteins, resulting in rapid internalization of these proteins [31, 32]. In ccRCC, up-regulation of ANKRD13D expression predicts poor prognosis [33]. Studies have shown that SOCS2 plays a role in many biological activities, such as cell apoptosis, proliferation, and inflammation [34, 35]. In ccRCC, SOCS2 may be a protective gene associated with immune cell infiltration [36]. CDKN1A is a potent cell cycle protein-dependent kinase inhibitor, and low CDKN1A is associated with a worse prognosis in patients with chromophobe renal cell carcinoma [37]. BAG2 has been reported to drive chemoresistance in breast cancer by exacerbating polymerization of mutant p53 [38], to promote hepatocellular carcinoma progression by activating P38/MAPK signaling [39]. Its role in ccRCC requires further research.

In addition, we performed enrichment analysis of differentially expressed genes in the two risk groups. The results suggest that these genes are involved in many signaling pathways that play key roles in tumor progression. For example, targeting cytokine-cytokine receptor interactions has been reported to prevent ulcerative colitis [40] and modulate the activation of naïve T cells [41]. Moreover, by analyzing the relationship between NRGS risk scores and TMB, we found that TMB was higher in the high-risk group compared to low-risk group. Tumorigenesis is a multi-step process in which oncogenic mutations in normal cells confer clonal dominance as an initial event. In general, the more mutations, the higher the degree of malignancy of the tumor, resulting in a poor prognosis for patients [42], which is further confirmed by our results (Fig. 3D). However, somatic cell mutations have been reported to be implicated in the generation of new antigens [43]. The production of neoantigens drives immune cell infiltration, which is associated with the sensitivity of cancer immunotherapy [44]. Therefore, high mutational burden in cellular genes produce new antigens, leading to changes in the level of immunocytes infiltration in tumor tissues, resulting in a better tumor response to immune checkpoint inhibitors and ultimately a better patient prognosis [45, 46]. Here, we found that the low-risk subgroup had lower levels of immune cell infiltration and immune checkpoint expression than the high-risk subgroup. Consistent with these results, an analysis of the IMvigor210 population showed that high-risk groups responded better to immunotherapy. Beyond immunotherapy, we evaluated the relationship of NRGS risk scores to drug response. These findings suggest that the drugs that are sensitive to patients in high-risk group are those that target signaling pathways like DNA replication and WNT, whereas in low-risk group are mainly targeting cell cycle, Chromatin histone acetylation, and RTK. These findings propose that NRGS may be able to provide new directions for treatment options for patients with ccRCC. However, athough we utilized multi-dimensional analysis with multi-omics data, there are some unavoidable limitations to our study. First, the number of validated datasets is limited. Although external validation was performed in a separate dataset, a large prospective multicenter study will be needed to test these discoveries in the future. Second, in our model, a more detailed basic experimental study of the underlying molecular mechanisms of Neddylation-related genes is necessary.

5 Conclusion

This study suggests that NRGs are associated with the development of ccRCC. This study utilizes bioinformatics methods to deepen our understanding of the function of NRGs in patients with ccRCC. On the basis of NRGs, we established a six-gene prognostic signature that performed well in predicting the prognosis of patients with ccRCC. Using the NRGS risk score, we can adjust the patient's treatment plan to some extent. This study may offer new insights into the search for prognostic biomarkers and the construction of therapeutic targets, which will be a valuable resource for further research.

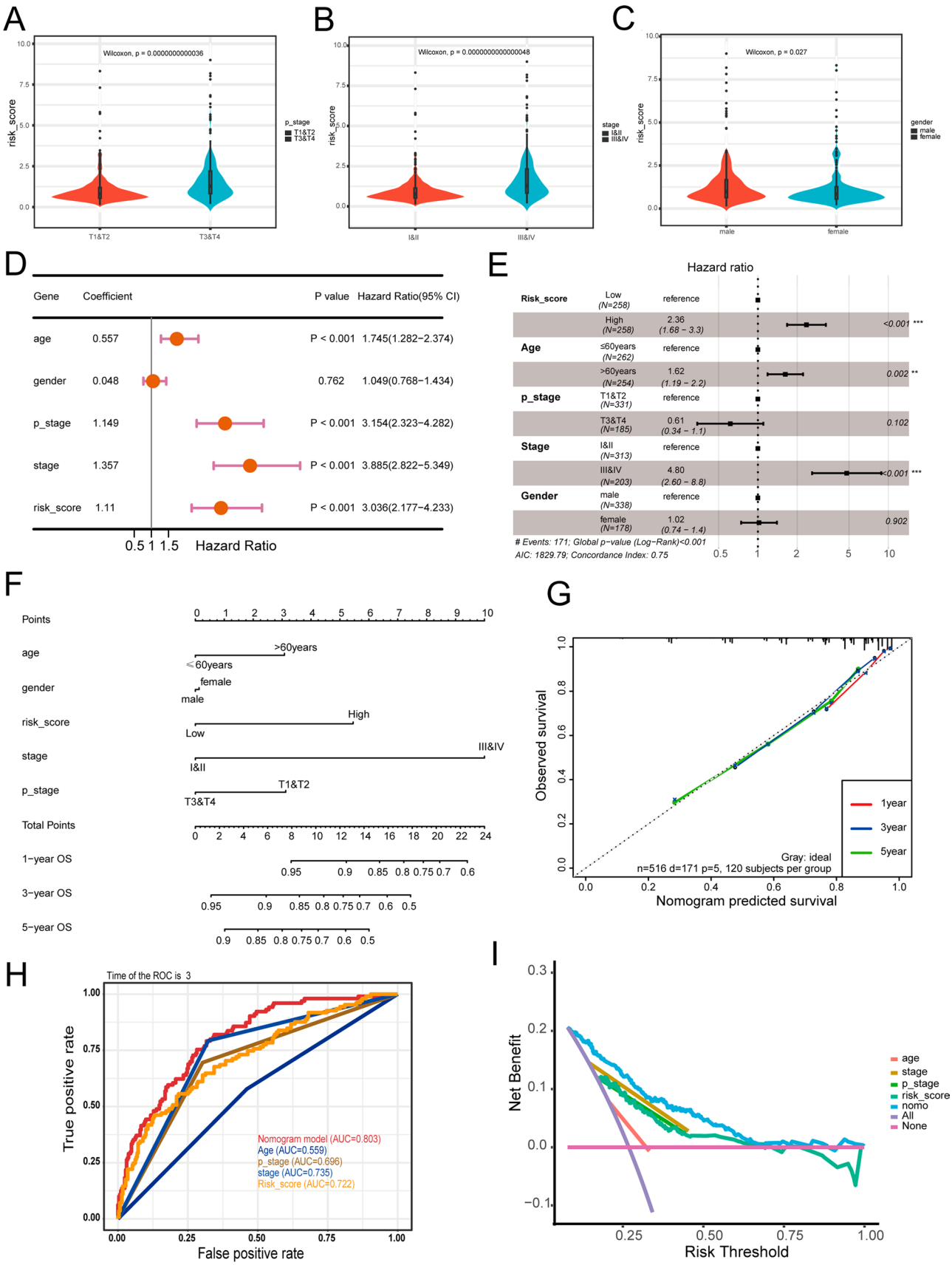
A
Wilcoxon, p = 0.0000000000036
risk_score
p_stage
T1&T2
T3&T4
B
Wilcoxon, p = 0.0000000000048
stage
I&II
III&IV
C
Wilcoxon, p = 0.027
gender
male
female
D
Gene Coefficient P value Hazard Ratio(95% CI)
age 0.557 P < 0.001 1.745(1.282−2.374)
gender 0.048 0.762 1.049(0.768−1.434)
p_stage 1.149 P < 0.001 3.154(2.323−4.282)
stage 1.357 P < 0.001 3.885(2.822−5.349)
risk_score 1.11 P < 0.001 3.036(2.177−4.233)
0.5 1 1.5 Hazard Ratio
E
Hazard ratio
Risk_score Low (N=258) reference
High (N=258) 2.36 (1.68 − 3.3) <0.001 ***
Age ≤60years (N=262) reference
>60years (N=254) 1.62 (1.19 − 2.2) 0.002 **
p_stage T1&T2 (N=331) reference
T3&T4 (N=185) 0.61 (0.34 − 1.1) 0.102
Stage I&II (N=313) reference
III&IV (N=203) 4.80 (2.60 − 8.8) <0.001 ***
Gender male (N=338) reference
female (N=178) 1.02 (0.74 − 1.4) 0.902
Events: 171; Global p−value (Log−Rank)<0.001
AIC: 1829.79; Concordance Index: 0.75
F
Points
age
gender
risk_score
stage
p_stage
Total Points
1−year OS
3−year OS
5−year OS
G
Observed survival
Nomogram predicted survival
1year
3year
5year
Gray: ideal
n=516 d=171 p=5, 120 subjects per group
H
Time of the ROC is 3
True positive rate
False positive rate
Nomogram model (AUC=0.803)
Age (AUC=0.559)
p_stage (AUC=0.696)
stage (AUC=0.735)
Risk_score (AUC=0.722)
I
Net Benefit
Risk Threshold
age
stage
p_stage
risk_score
nomo
All
None

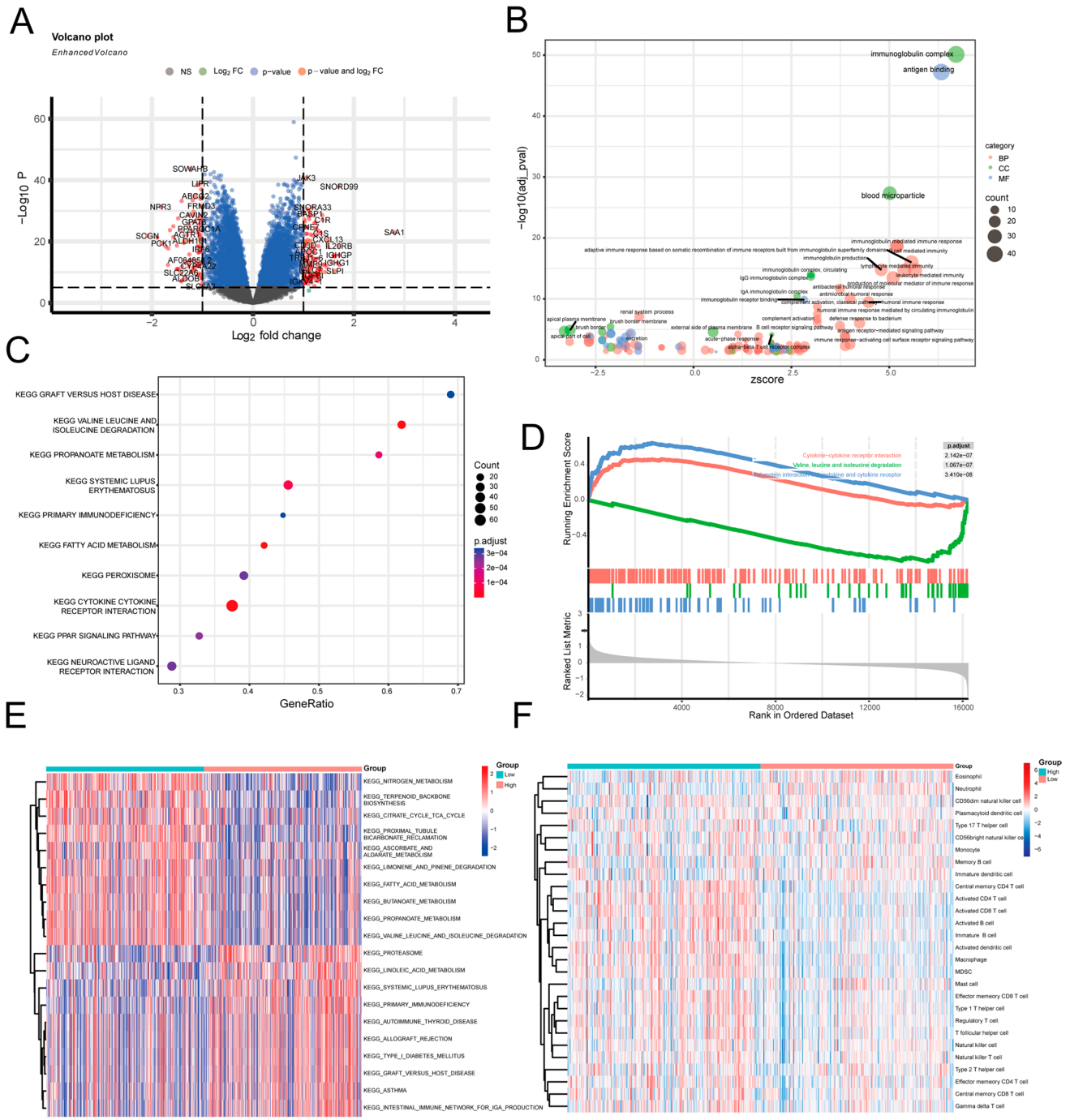

Fig. 5 Functional enrichment analysis between Risk Types. **A** Volcano plot of DEGs between high- and low-risk groups. Dotplot showing GO terms (**B**) and KEGG pathways (**C**) of differentially expressed genes between different risk types. **D** GSEA results between high-risk and low-risk groups. **E** The heatmap shows KEGG pathway analysis of GSVA in two subgroups. **F** The ssGSEA analysis of the immune cell infiltration level in the two subgroups

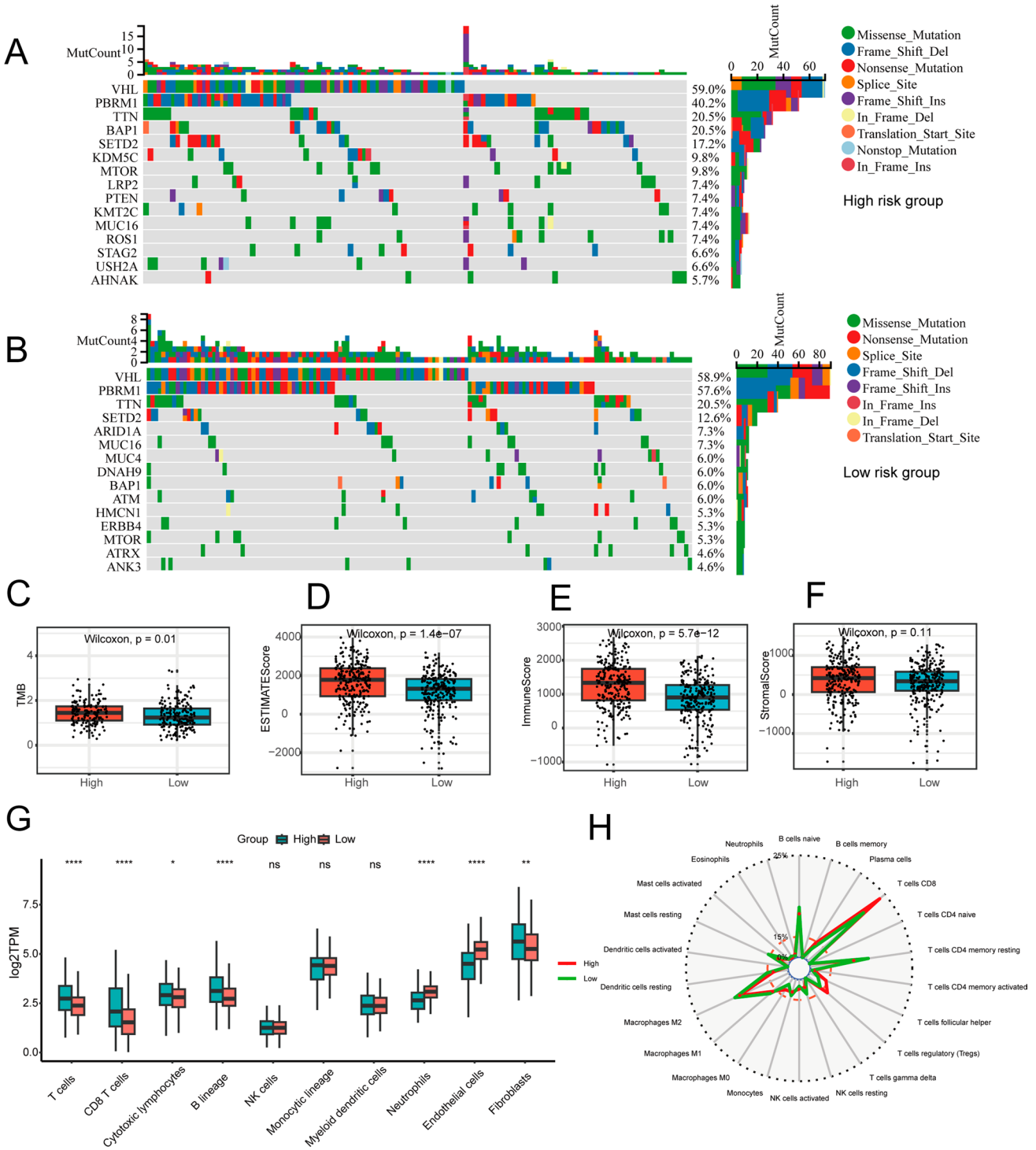

Fig. 6 Mutation frequency and immune cell infiltration in ccRCC patients in the TCGA database. Waterfall plot of the top 15 somatic mutation signatures for groups with high (**A**) and low (**B**) NRGs risk scores. **C** TMB between the low- and high-risk subgroups based on NRGS. Correlations between NRG risk score and both Estimate (**D**), immune (**E**) and stromal scores (**F**). MCPcounter (**G**) and CIBERSORT (**H**) were used to analyze the degree of immune cell infiltration in the two groups (ns, not significant; *$P < 0.05$; **$P < 0.01$; ***$P < 0.001$; ****$P < 0.001$)

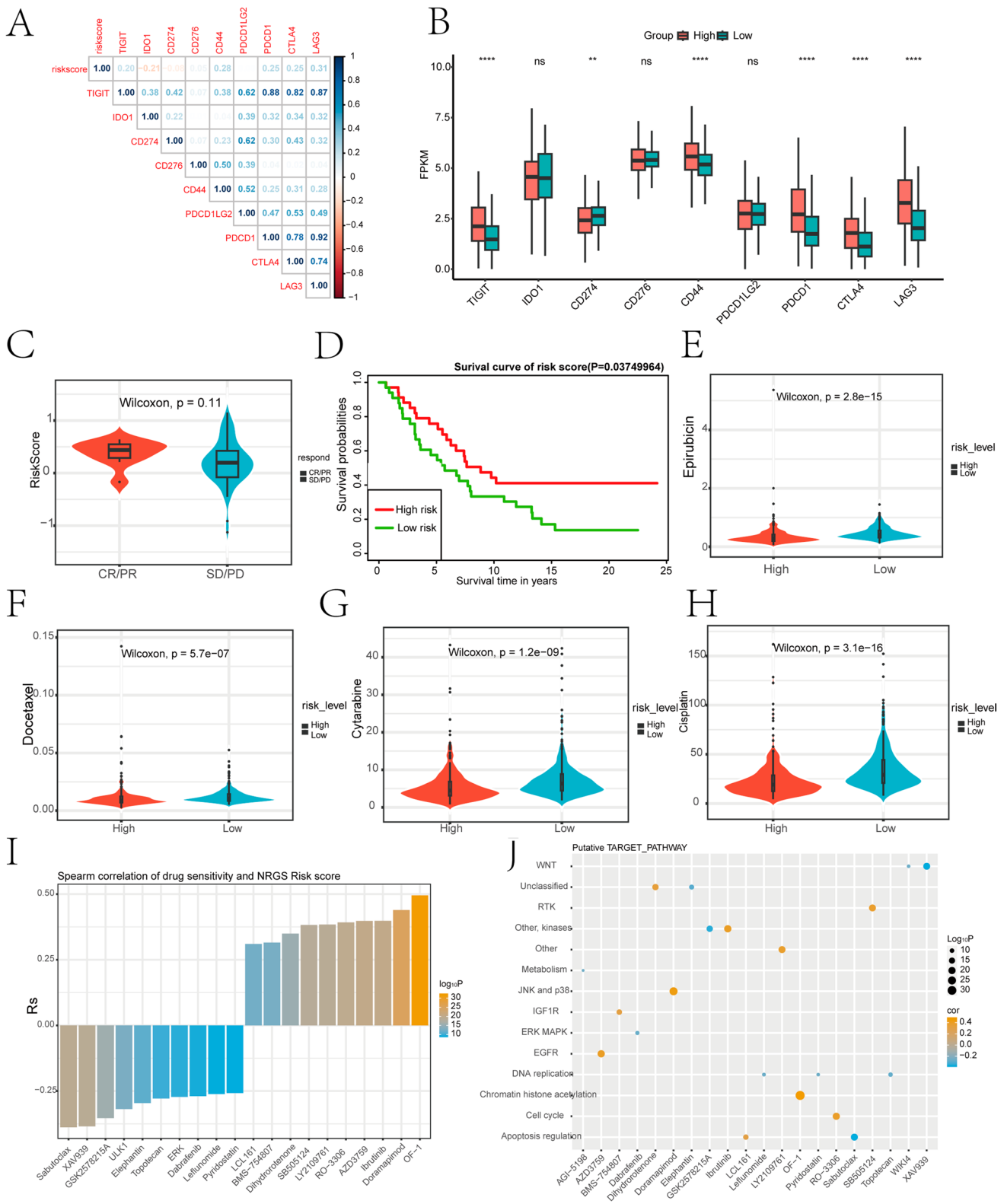

Fig. 7 Relationship between NRGS risk score and immune response and drug sensitivity. **A** Correlation analysis of Immune checkpoints and NRGS risk score. **B** Differences in immune checkpoint genes between high- and low-risk groups. **C** Risk score level between CR/PR and SD/PD group. **D** KM curves for high/low risk types of kidney cancer based on the IMvigor210 cohort. IC50 of **E** Epirubicin, **F** Docetaxel, **G** Cytarabine, and **H** Cisplatin between different NRG risk groups. **I** The correlation between NRGS risk score and drug sensitivity (AUC values of GDSC) examined by the Spearman analysis. **J** Putative targets or functional pathways of the drugs that are sensitivity to the NRGS risk score (*ns* not significant; $^{**}P < 0.01$; $^{****}P < 0.001$)

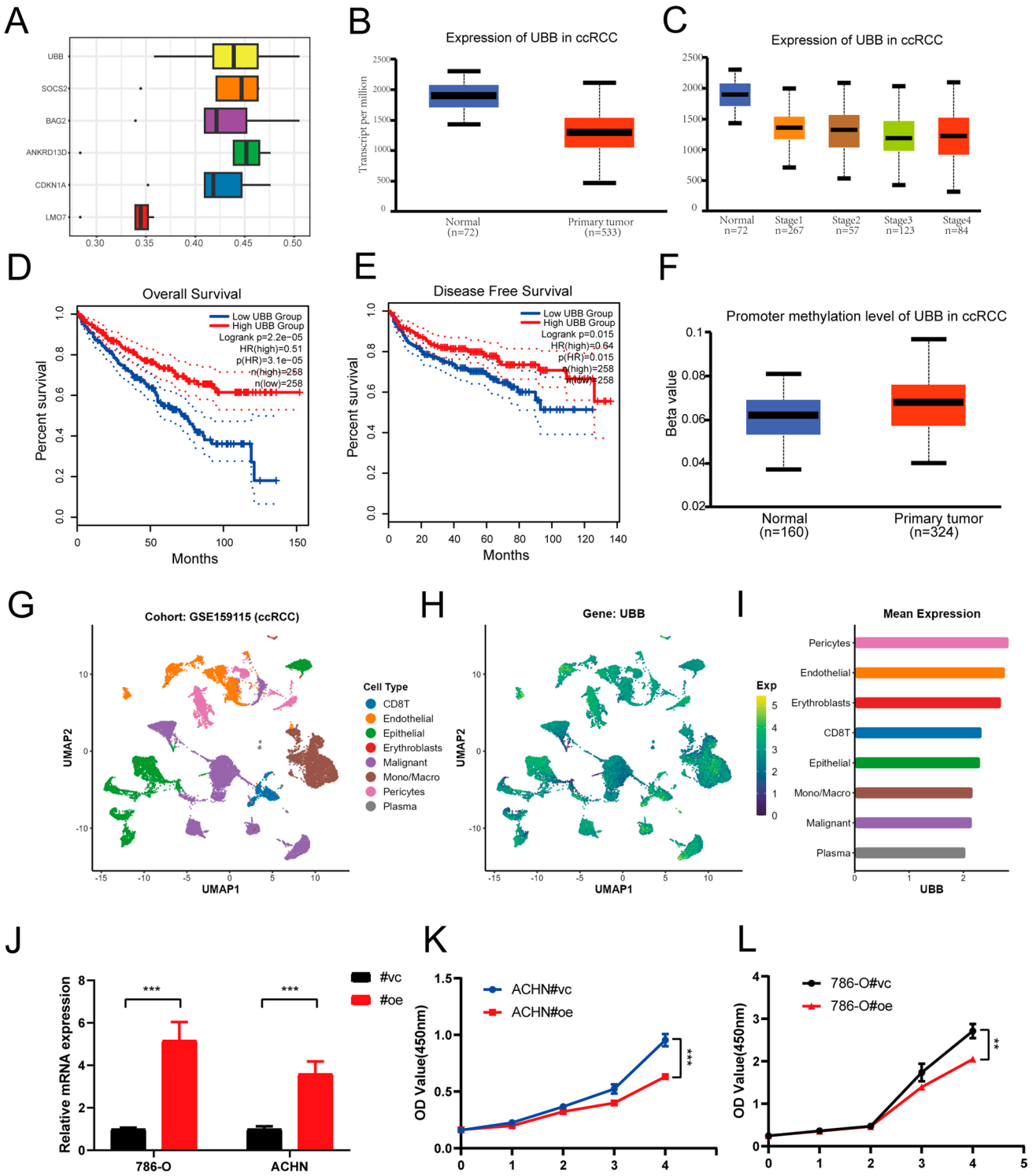

Fig. 8 Identifying the hub gene of NRGS. **A** The "mgeneSim" function reveals the hub gene UBB in the NRGS. **B** The boxplot shows the UBB expression level among renal cancer, normal tissues and **C** different tumor stages. **D**, **E** K-M plot show the overall and DFS survival possibility between high and low level of UBB. **F** Promoter methylation level of UBB in ccRCC. **G**, **I** UMAP and barplot plot show the expression of UBB in different cell types. **J** RT-qPCR demonstrates the overexpression efficiency of UBB. (K&L) CCK8 shows proliferation of RCC after overexpression of UBB

Acknowledgements This work was financed by grants from the Science and Technology Plan Project of Guangzhou (No.202201020562) and Guangzhou Postdoctoral Startup Fund (2022-2025).

Author contributions Conceptualization: G.X.C and C.S.R; methodology: L.Y.P. and X.X.H.; investigation and analysis: C.S.R M.Z.H. and W.Y.S; visualization: C.S.R.; writing original draft: C.S.R. and G.X.C; writing review and editing: G.X.C and C.S.R.; funding acquisition and project administration: G.X.C.

Funding This work was financed by grants from the Science and Technology Plan Project of Guangzhou (No.202201020562) and Guangzhou Postdoctoral Startup Fund (2022-2025).

Data availability The data used in this study could be obtained at (https://www.cancer.gov; http://www.ncbi.nlm.nih.gov/geo; https://www.genecards.org; https://www.ebi.ac.uk/) and the code is available from the corresponding author on reasonable request.

Declarations

Ethics approval and consent to participate Not applicable.

Competing interests The authors declare no competing interests.

References

1. Siegel RL, Giaquinto AN, Jemal A. Cancer statistics, 2024. CA Cancer J Clin. 2024;74:12–49.
2. Hsieh JJ, Purdue MP, Signoretti S, Swanton C, Albiges L, Schmidinger M, et al. Renal cell carcinoma. Nat Rev Dis Primers. 2017;3:1–19.
3. Li Y, Lih T-SM, Dhanasekaran SM, Mannan R, Chen L, Cieslik M, et al. Histopathologic and proteogenomic heterogeneity reveals features of clear cell renal cell carcinoma aggressiveness. Cancer Cell. 2023;41:139-163.e17.
4. Rouprêt M, Seisen T, Birtle AJ, Capoun O, Compérat EM, Dominguez-Escrig JL, et al. European Association of Urology Guidelines on upper urinary tract urothelial carcinoma: 2023 update. Eur Urol. 2023;84:49–64.
5. Motzer RJ, Jonasch E, Agarwal N, Alva A, Bagshaw H, Baine M, et al. NCCN Guidelines® insights: kidney cancer, Version 2.2024. J Natl Compr Canc Netw. 2024;22:4–16.
6. Alchahin AM, Mei S, Tsea I, Hirz T, Kfoury Y, Dahl D, et al. A transcriptional metastatic signature predicts survival in clear cell renal cell carcinoma. Nat Commun. 2022;13:5747.
7. Fuentes-Antrás J, Alcaraz-Sanabria AL, Morafraile EC, Noblejas-López MDM, Galán-Moya EM, Baliu-Pique M, et al. Mapping of genomic vulnerabilities in the post-translational ubiquitination, SUMOylation and neddylation machinery in breast cancer. Cancers. 2021;13:833.
8. Pan S, Chen R. Pathological implication of protein post-translational modifications in cancer. Mol Aspects Med. 2022;86: 101097.
9. Mao H, Lin X, Sun Y. Neddylation regulation of immune responses. Research (Wash D C). 2023;6:0283.
10. Zhou Q, Zheng Y, Sun Y. Neddylation regulation of mitochondrial structure and functions. Cell Biosci. 2021;11:55.
11. Xia X, Hu T, He X, Liu Y, Yu C, Kong W, Liao Y, Tang D, Liu J, Huang H. Neddylation of HER2 inhibits its protein degradation and promotes breast cancer progression. Int J Biol Sci. 2023;19(2):377–92. https://doi.org/10.7150/ijbs.75852.
12. Zhou Q, Lin W, Wang C, Sun F, Ju S, Chen Q, Wang Y, Chen Y, Li H, Wang L, Hu Z, Jin H, Wang X, Sun Y. Neddylation inhibition induces glutamine uptake and metabolism by targeting CRL3SPOP E3 ligase in cancer cells. Nat Commun. 2022;13(1):3034. https://doi.org/10.1038/s41467-022-30559-2.
13. Shapiro DD, Zacharias NM, Tripathi DN, Karki M, Bertocchio JP, Soeung M, He R, Westerman ME, Gao J, Rao P, Lam TNA, Jonasch E, Perelli L, Cheng EH, Carugo A, Heffernan TP, Walker CL, Genovese G, Tannir NM, Karam JA, Msaouel P. Neddylation inhibition sensitises renal medullary carcinoma tumours to platinum chemotherapy. Clin Transl Med. 2023;13(5):1267. https://doi.org/10.1002/ctm2.1267.
14. Wu MH, Lee CY, Huang TJ, Huang KY, Tang CH, Liu SH, Kuo KL, Kuan FC, Lin WC, Shi CS. MLN4924, a protein Neddylation inhibitor, suppresses the growth of human chondrosarcoma through inhibiting cell proliferation and inducing endoplasmic reticulum stress-related apoptosis. Int J Mol Sci. 2018;20(1):72.
15. Wu T, Hu E, Xu S, Chen M, Guo P, Dai Z, et al. clusterProfiler 4.0: A universal enrichment tool for interpreting omics data. Innovation (N Y). 2021;2:100141.
16. Wilkerson MD, Hayes DN. ConsensusClusterPlus: a class discovery tool with confidence assessments and item tracking. Bioinformatics. 2010;26:1572–3.
17. Yang W, Soares J, Greninger P, Edelman EJ, Lightfoot H, Forbes S, et al. Genomics of Drug Sensitivity in Cancer (GDSC): a resource for therapeutic biomarker discovery in cancer cells. Nucleic Acids Res. 2013;41:D955-961.

18. Maeser D, Gruener RF, Huang RS. oncoPredict: an R package for predicting in vivo or cancer patient drug response and biomarkers from cell line screening data. Brief Bioinform. 2021;22:bbab260.
19. Shen W, Song Z, Zhong X, Huang M, Shen D, Gao P, et al. Sangerbox: a comprehensive, interaction-friendly clinical bioinformatics analysis platform. iMeta. 2022;1:e36.
20. Yu G, Li F, Qin Y, Bo X, Wu Y, Wang S. GOSemSim: an R package for measuring semantic similarity among GO terms and gene products. Bioinformatics. 2010;26:976–8.
21. Wang J, Zhao E, Geng B, Zhang W, Li Z, Liu Q, et al. Downregulation of UBB potentiates SP1/VEGFA-dependent angiogenesis in clear cell renal cell carcinoma. Oncogene. 2024;43:1386–96.
22. Barata PC, Rini BI. Treatment of renal cell carcinoma: Current status and future directions. CA Cancer J Clin. 2017;67:507–24.
23. Kim SP, Alt AL, Weight CJ, Costello BA, Cheville JC, Lohse C, et al. Independent validation of the 2010 American Joint Committee on Cancer TNM classification for renal cell carcinoma: results from a large, single institution cohort. J Urol. 2011;185:2035–9.
24. Xu J, Zhang W, Tong J, Liu C, Zhang Q, Cao L, et al. A phase I trial of autologous RAK cell immunotherapy in metastatic renal cell carcinoma. Cancer Immunol Immunother. 2024;73:107.
25. Huang H, Chen K, Zhu Y, Hu Z, Wang Y, Chen J, et al. A multi-dimensional approach to unravel the intricacies of lactylation related signature for prognostic and therapeutic insight in colorectal cancer. J Transl Med. 2024;22:211.
26. Luo X, Wang Y, Zhang H, Chen G, Sheng J, Tian X, et al. Identification of a prognostic signature for ovarian cancer based on ubiquitin-related genes suggesting a potential role for FBXO9. Biomolecules. 2023;13:1724.
27. Zhen Y-Y, Wu C-H, Chen H-C, Chang EE, Lee J-J, Chen W-Y, et al. Coordination of LMO7 with FAK signaling sustains epithelial integrity in renal epithelia exposed to osmotic pressure. Cells. 2022;11:3805.
28. Duan S, Lou X, Chen S, Jiang H, Chen D, Yin R, et al. Macrophage LMO7 deficiency facilitates inflammatory injury via metabolic-epigenetic reprogramming. Acta Pharm Sin B. 2023;13:4785–800.
29. Dubois M-L, Meller A, Samandi S, Brunelle M, Frion J, Brunet MA, et al. UBB pseudogene 4 encodes functional ubiquitin variants. Nat Commun. 2020;11:1306.
30. Han B, Jung B-K, Park S-H, Song KJ, Anwar MA, Ryu K-Y, et al. Polyubiquitin gene Ubb is required for upregulation of Piwi protein level during mouse testis development. Cell Death Discov. 2021;7:194.
31. Won M, Park KA, Kim S, Ju E, Ko Y, Yoo H, et al. ANKRD13a controls early cell-death checkpoint by interacting with RIP1 independent of NF-κB. Cell Death Differ. 2022;29:1152–63.
32. Mattioni A, Boldt K, Auciello G, Komada M, Rappoport JZ, Ueffing M, Castagnoli L, Cesareni G, Santonico E. Ring Finger Protein 11 acts on ligand-activated EGFR via the direct interaction with the UIM region of ANKRD13 protein family. FEBS J. 2020;287(16):3526–50. https://doi.org/10.1111/febs.15226.
33. Zhou W, Huang Y, Liu J, Liu Y, Liu Y, Yu C. Identification of ANKRD13D as a potential target in renal cell carcinomas. Int J Biol Markers. 2024;39(2):149–57.
34. Chen Q, Zheng W, Guan J, Liu H, Dan Y, Zhu L, et al. SOCS2-enhanced ubiquitination of SLC7A11 promotes ferroptosis and radiosensitization in hepatocellular carcinoma. Cell Death Differ. 2023;30:137–51.
35. Li S, Han S, Jin K, Yu T, Chen H, Zhou X, et al. SOCS2 suppresses inflammation and apoptosis during NASH progression through limiting NF-κB activation in macrophages. Int J Biol Sci. 2021;17:4165–75.
36. Li C, Zhang W, Fang T, Li N, Wang Y, He L, et al. Identification of the prognostic value among suppressor of cytokine signaling family members in kidney renal clear cell carcinoma. Front Mol Biosci. 2021;8: 585000.
37. Ohashi R, Angori S, Batavia AA, Rupp NJ, Ajioka Y, Schraml P, et al. Loss of CDKN1A mRNA and protein expression are independent predictors of poor outcome in chromophobe renal cell carcinoma patients. Cancers (Basel). 2020;12:465.
38. Huang X, Shi D, Zou X, Wu X, Huang S, Kong L, et al. BAG2 drives chemoresistance of breast cancer by exacerbating mutant p53 aggregate. Theranostics. 2023;13:339–54.
39. Zhang X, Dong K, Zhang J, Kuang T, Luo Y, Yu J, et al. GNB1 promotes hepatocellular carcinoma progression by targeting BAG2 to activate P38/MAPK signaling. Cancer Sci. 2023;114:2001–13.
40. Li Y, Tian Y-Y, Wang J, Lin R, Zhang Y, Zhang M-M, et al. Main active components of *Ilex rotunda* Thunb. protect against ulcerative colitis by restoring the intestinal mucosal barrier and modulating the cytokine-cytokine interaction pathways. J Ethnopharmacol. 2024;318:116961.
41. Jaeger-Ruckstuhl CA, Lo Y, Fulton E, Waltner OG, Shabaneh TB, Simon S, et al. Signaling via a CD27-TRAF2-SHP-1 axis during naive T cell activation promotes memory-associated gene regulatory networks. Immunity. 2024;57:287-302.e12.
42. Xavier CB, Lopes CDH, Awni BM, Campos EF, Alves JPB, Camargo AA, et al. Interplay between tumor mutational burden and mutational profile and its effect on overall survival: a pilot study of metastatic patients treated with immune checkpoint inhibitors. Cancers (Basel). 2022;14:5433.
43. Sholl LM, Hirsch FR, Hwang D, Botling J, Lopez-Rios F, Bubendorf L, et al. The promises and challenges of tumor mutation burden as an immunotherapy biomarker: a perspective from the International Association for the Study of Lung Cancer Pathology Committee. J Thorac Oncol. 2020;15:1409–24.
44. Yang S, Liu T, Cheng Y, Bai Y, Liang G. Immune cell infiltration as a biomarker for the diagnosis and prognosis of digestive system cancer. Cancer Sci. 2019;110:3639–49.
45. McGrail DJ, Pilié PG, Rashid NU, Voorwerk L, Slagter M, Kok M, Jonasch E, Khasraw M, Heimberger AB, Lim B, Ueno NT, Litton JK, Ferrarotto R, Chang JT, Moulder SL, Lin SY. High tumor mutation burden fails to predict immune checkpoint blockade response across all cancer types. Ann Oncol. 2021;32(5):661–72. https://doi.org/10.1016/j.annonc.2021.02.006.
46. Cui S, Feng J, Tang X, Lou S, Guo W, Xiao X, et al. The prognostic value of tumor mutation burden (TMB) and its relationship with immune infiltration in breast cancer patients. Eur J Med Res. 2023;28:90.